Journal of Experimental and Theoretical Physics, Vol. 98, No. 4, 2004, pp. 719–727.
Translated from Zhurnal Éksperimental'noĭ i Teoreticheskoĭ Fiziki, Vol. 125, No. 4, 2004, pp. 821–830.

PLASMA, GASES

Thermodynamics and Correlation Functions of an Ultracold Nonideal Rydberg Plasma

M. Bonitz[a], B. B. Zelener[b,*], B. V. Zelener[b], É. A. Manykin[c], V. S. Filinov[d], and V. E. Fortov[d]

[a]*Lehrstuhl Statistische Physik, Institut für Teoretische Physik und Astrophysik, Christian-Albrechts-Universität Kiel, Kiel, D-24098 Germany*

[b]*Joint Institute for High Temperatures, Russian Academy of Sciences, Moscow, 125412 Russia*

[c] *Russian Research Centre Kurchatov Institute, Moscow, 123182 Russia*

[d]*Institute of Thermal Physics of Extreme States, Joint Institute for High Temperatures, Russian Academy of Sciences, Moscow, 125412 Russia*

**e-mail: bobozel@mail.ru*

Received October 2, 2003

Abstract—A pseudopotential model is suggested to describe the thermodynamics and correlation functions of an ultracold, strongly nonideal Rydberg plasma. The Monte Carlo method is used to determine the energy, pressure, and correlation functions in the ranges of temperatures $T = 0.1$–10 K and densities $n = 10^{-2}$–10^{16} cm^{-3}. For a weakly nonideal plasma, the results closely agree with the Debye asymptotic behavior. For a strongly nonideal plasma, many-particle clusters and a spatial order in the arrangement of plasma electrons and ions have been found to be formed. © *2004 MAIK "Nauka/Interperiodica".*

1. INTRODUCTION

The unique experimental works [1–3] have given us an insight into some of the physical properties of a dense ionized gas at cryogenic temperatures. Until now, a dense ionized gas has been traditionally produced at high temperatures and high pressures.

In [1–3], in which a Xe plasma was studied, about 5×10^6 metastable Xe atoms (the $6S[3/2]_2$ level, a lifetime of 43 s) were produced, decelerated by using the Zeeman technique, collected in a magneto-optical trap, and radiatively cooled on the $6S[3/2]_2$ –$6P[5/2]_3$ ($\lambda_1 \approx$ 882 nm) transition down to a temperature of 100 μK. The maximum atomic density reached 5×10^{10} cm^{-3}; the density distribution was Gaussian with a root-mean-square radius of $\sigma \approx 180$ μm.

To produce a plasma, more than 20% of the atoms were photoionized over 10 ns. First, the $6P[5/2]_3$ ($\lambda_1 \approx$ 882 nm) level was populated, and then the atom was ionized by photons with a wavelength $\lambda_2 \approx 514$ nm. The difference between the photon energy and the ionization potential, ΔE, was distributed between electrons and ions. Because of the small electron-to-ion mass ratio, only an energy of $4 \times 10^{-6}\Delta E$ was acquired by ions, while the remaining energy was acquired by electrons. In [1–3], $\Delta E/k$ was varied in a controllable way between 0.1 and 1000 K. The maximum charged particle density was

$$n = n_e + n_i = 2 \times 10^9 \text{ cm}^{-3}.$$

An anomalous slowdown of the recombination in the produced plasma was found in [1–3]. The recombination time was on the order of 100 μs. The recombination time estimated by using a formula valid for a rarefied plasma is several nanoseconds, which is many orders of magnitude shorter than the observed value.

Note that the produced plasma is strongly nonideal. In this plasma, the ratio of the mean potential energy of the particles to their kinetic energy (nonideality parameter), $\gamma = \beta e^2 n^{1/3}$ (where $\beta = 1/kT$ is the inverse temperature, and e is the electron charge), is much larger than unity. Thus, at $T = 0.1$ K and $n = 2 \times 10^9$ cm^{-3}, $\gamma = 21$. At the same time, the electrons in this plasma are nondegenerate. The ratio of the thermal de Broglie wavelength $\lambda\!\!\!^{-}_e$ of an electron to the mean particle separation (degeneracy parameter) at $T = 0.1$ K and $n = 2 \times 10^9$ cm^{-3} is much smaller than unity:

$$n^{1/3}\lambda\!\!\!^{-}_e = \frac{n^{1/3}\hbar}{\sqrt{2m_e kT}} = 0.2 \times 10^{-2}. \quad (1)$$

Here, m_e is the electron mass, and $\hbar$ is the Planck constant.

In a strongly nonideal plasma, the estimates of any processes based on the formulas obtained in the approximation of $\gamma \ll 1$ are inapplicable for such nonideality parameters γ.

2. THERMAL RELAXATION

Based on the properties of a nonideal plasma [4], the authors of [1–3] concluded that thermal equilibrium sets in several tens of microseconds. It seems to us that this conclusion is unjustified, because a weakly nonideal plasma with $\gamma \ll 1$ was considered in [4]. Since there is no quantitative kinetic theory for $\gamma \geq 1$, only qualitative estimates can be obtained. In this case, it follows from general physical considerations that the thermal relaxation time in a strongly coupled system (e.g., at fixed temperature T with variation in particle density n) will be shorter than that in a weakly coupled system.

To estimate the thermal relaxation time in a gas of electrons and ions, we use a standard expression from [5] for $\gamma \ll 1$ and $n\lambda^3 \ll 1$:

$$\tau_{ei}^{\varepsilon} = \frac{T_e^{3/2} M}{8 n_i z^2 e^4 (2\pi m_e)^{1/2}} \frac{1}{L_e}. \quad (2)$$

Here, T_e is the electron temperature, M is the ion mass, z is the ion charge, n_i is the ion density, and L_e is the Coulomb logarithm:

$$L_e = \ln\left(\frac{aT_e}{ze^2}\right) = \ln\frac{1}{\sqrt{\pi\gamma^{3/2}}} \quad \left(\frac{ze^2}{\hbar v_{Te}} \gg 1\right), \quad (3)$$

where v_{Te} is the electron velocity that corresponds to T_e, and

$$a = \frac{1}{\sqrt{4\pi n_e \beta e^2}} \quad (4)$$

is the Debye screening length.

If the plasma is electrically neutral, then $n_e = n_i$. Formula (2) contains a Coulomb logarithm L_e that has no physical meaning for $\gamma \geq 1$. The Coulomb logarithm L_e arises in this formula when the transport cross section is calculated. The latter is generally determined in the rarefied case for $a \geq \bar{n}$ (where $\bar{n}$ is the mean density). However, it is clear that the transport cross section always has a physical meaning and is finite.

By analogy, the estimate of the thermal relaxation time τ_{ei}^{ε} for $\gamma \geq 1$ can be represented by using the characteristic physical quantities as (2); in this case, however, L_e^* (the effective Coulomb logarithm that includes the collective effects in a nonideal plasma) should be substituted for L_e:

$$\tau_{ei}^{\varepsilon} = \frac{(\tau_{ei}^{\varepsilon})_0}{L_e^*}, \quad (5)$$

where

$$(\tau_{ei}^{\varepsilon})_0 = \frac{T_e^{3/2} M}{8 n_i z^2 e^4 (2\pi m_e)^{1/2}},$$

$(\tau_{ei}^{\varepsilon})_0 = 3.4 \times 10^{-2}$ s at $T_e = 0.1$ K and $n_i = 10^4$, $z = 1$ ($\gamma = 0.67$, $M = 131.3$ amu). At $T_e = 0.1$ K and $n_i = 10^{10}$, $(\tau_{ei}^{\varepsilon})_0 = 34$ ns.

We also assume that the differential scattering cross section remains Coulomb, but either corrections to it arise or the integration limits change. However, the dependence of the relaxation time on n at $T = \text{const}$ remains logarithmic.

The value of τ_{ei}^{ε} can change via the substitution of L_e^* for L_e by no more than a factor of 10 to 20. Of course, all of this reasoning must be confirmed by rigorous estimations or numerical calculations. Thus, we may assume that thermal equilibrium at $T = 0.1$ K and $n = 10^9$–10^{10} sets in less than 1 μs.

3. THEORETICAL APPROACHES TO STUDYING AN ULTRACOLD NONIDEAL RYDBERG PLASMA

The Xe plasma produced in the experiments [1–3] consists of singly charged Xe ions, electrons, and highly excited ($n > 100$) hydrogen-like Xe states. These states are called Rydberg atoms. The possibility of the existence of condensed excited states of matter was first considered in [6]. At present, these condensed states of substance for Rydberg atoms (the so-called Rydberg substance) have been extensively studied theoretically [7, 8] and experimentally [9–11]. Subsequently, this idea has been developed by several authors (see the review [12]). According to this approach, the interaction between Rydberg atoms as their density increases ultimately leads to a change in the phase state of the system and to a qualitative change in all parameters. Moreover, in contrast to free Rydberg atoms whose lifetime in an excited state is about 10 ns, the lifetime of a Rydberg substance is macroscopically long. Despite the low density that is the gas density by its parameters, the condensed excited state is a metastable ordered state of the substance. At present, there are experimental data [13, 14] for a cesium plasma at $T = 500$–1000 K that suggest the existence of a Rydberg substance.

In [15, 16], the experimental data [13, 14] were found to correlate with the ideas of an isolated region of metastable states of an ultracold nonideal plasma. In [6, 12], the methods of solid-state physics were used to produce a Rydberg substance by assuming the presence of an electron Fermi liquid. In [17, 18], the recombination time of a dense plasma was calculated numerically and was shown to be much longer than that for a

weakly nonideal plasma. The authors of [19, 20] suggested a different approach to studying the thermodynamics of a Rydberg substance in the case where the electron gas is nondegenerate. This approach uses previously developed methods for a strongly nonideal nondegenerate plasma [21].

We consider the thermodynamic equilibrium of a nonideal gas of electrons and ions ($\gamma \geq 1$). This gas is peculiar in that there is absolutely no atomic discrete spectrum or there are discrete states with $n \geq n^*$, where $n^* = 100$ or more. Since $n^* \geq 100$, the states may be said to be Rydberg ones. Strictly speaking, there is no full thermodynamic equilibrium in our case. Therefore, when we talk about thermodynamic equilibrium degrees of freedom, we primarily have in mind the translational degrees of freedom. The thermodynamic equilibrium of all the remaining degrees of freedom (rotational, vibrational, dissociation and chemical reactions, ionization and electron excitation) arises much later. It may be assumed that in easily excited degrees of freedom, equilibrium exists at each instant of time, while the slow relaxation processes do not proceed at all over the period under consideration. We will use results from [21–29] to describe this gas.

4. THE PSEUDOPOTENTIAL MODEL AND THE RANGE OF ITS APPLICABILITY

The thermodynamics of an equilibrium quantum-mechanical system is completely determined if the partition function is known:

$$Z_N \approx \mathrm{Tr}(\exp(-\beta\hat{H})) = \int_{V^N} \sum_{n=1}^{\infty} |\psi_n|^2 \exp(-\beta E_n) dq_N, \quad (6)$$

where $\mathrm{Tr}(\exp(-\beta\hat{H}))$ is the trace of the density matrix $\exp(-\beta\hat{H})$; $\psi_n(q_N)$ and E_n are the wave functions and energy levels of N particles, respectively; $\hat{H}$ is the Hamiltonian of the N-particle system; q_N are the coordinates of the N particles; and V is the volume of the system.

The authors of [25–29] developed an approach that allows the thermodynamic properties of a dense plasma to be described over a wide range of nonideality and degeneracy parameters, including the region of strong nonideality and degeneracy. However, a simpler approach developed in [21–24] can be used for a nondegenerate plasma. The authors of these papers suggested a pseudopotential model to calculate the partition function of a nonideal nondegenerate plasma. It involves the Slater partition function

$$S_N = N!\lambda^{3N} \sum_{n=1}^{\infty} |\psi_n|^2 \exp(-\beta E_n), \quad (7)$$

where λ is the particle thermal wavelength.

The essence of the pseudopotential model is that the partition function (7) is represented as a product of the pair electron–electron, ion–ion, and electron–ion Slater partition functions:

$$S_{N_e+N_i} = \prod_{i<j=1}^{2N} S_{ij} = \prod_{i<j=1}^{N_e} S_{ee} \times \prod_{i<j=1}^{N_i} S_{ii} \prod_{i<j=1}^{N=N_i=N_e} S_{ei}. \quad (8)$$

In the experimental conditions under consideration, this approximation is valid not only for $\gamma < 1$, but also for $\gamma \geq 1$, because there are neither pair nor many-particle bound states in the Xe gas. By analogy with the classical case, product (8) may be substituted with

$$S_{N_i+N_e} = \exp\left(-\beta \sum_{ij} U_{ij}\right), \quad (9)$$

where

$$U_{ij} = -\frac{\ln S_{ij}}{\beta} \quad (10)$$

is the pseudopotential.

The pair Slater partition functions for electron–ion, electron–electron, and ion–ion interactions can be calculated accurately. The expression for the long-range pseudopotential is identical to the Coulomb law, while the short-range pseudopotential is finite and temperature-dependent.

4.1. The Electron–Ion Pseudopotential

For the interaction of an electron with an ion, the pseudopotential Φ_{ei} is defined by the relation

$$\exp(-\beta\Phi_{ei}(r, T)) = S_{ei} = 8\pi^{3/2}\lambda_{ei}^3 \sum_{E_\alpha = E_0}^{\infty} |\Psi_\alpha(r)|^2 \exp(-\beta E_\alpha), \quad (11)$$

where S_{ei} is the two-particle Slater partition function, $E_\alpha(r)$ is the energy of the electron in the field of the ion

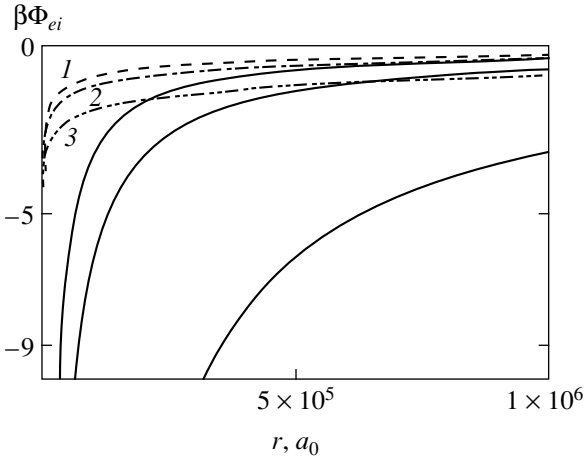

Fig. 1. The ion–electron pseudopotentials at various temperatures, $T = 1$ (*1*), 0.5 (*2*), and 0.1 K (*3*), compared to the Coulomb potentials (solid lines)

in state α, $\Psi_\alpha(r)$ is the corresponding wave function, and $\lambda_{ei} = \lambda_e/\sqrt{2}$. The summation is over all possible states E_α. This pseudopotential is finite at $r = 0$, while the expression for the long-range pseudopotential is identical to the Coulomb law.

For a plasma without bound states up to $n = n_0$, the expression for $S_{ei}(r, T)$ can be written as [21]

$$S_{ei}(r, T) = S_d + S_c. \tag{12}$$

Here,

$$S_d = 8\pi^{3/2}\lambda_{ei}^3 \sum_{E_\alpha = E_0}^{E'} |\psi_\alpha(r)|^2 \exp(-\beta E_\alpha) \tag{13}$$

is the contribution of the part of the discrete spectrum from E_0 to E', which can be calculated from the known wave functions $\Psi_\alpha(r)$ for the hydrogen atom, and the contribution of the remaining part of the spectrum is

$$S_c(z, T) = \exp\left(-\frac{\beta e^2}{r}\right), \tag{14a}$$

if

$$\frac{\beta E' r}{\lambda_{ei}} \geq \frac{|\beta e^2|}{\lambda_{ei}},$$

and

$$S_c(r, T) = \left[1 - y\left(\sqrt{\beta E' + \frac{\beta e^2}{r}}\right)\right]\exp\left(-\frac{\beta e^2}{r}\right) + 2\pi^{-1/2}\left(\beta E' + \frac{\beta e^2}{r}\right)^{1/2}, \tag{14b}$$

if

$$\frac{\beta E' r}{\lambda_{ei}} < \frac{|\beta e^2|}{\lambda_{ei}},$$

where

$$y(z) = 2\pi^{-1/2}\int_0^z \exp(-t^2)dt.$$

The partition function $S_c(r, T)$ was derived in the quasi-classical approximation for bound states at $E_\alpha > E'$ and continuum states.

Expressions (13) and (14) for $|\beta e^2/\lambda_{ei}| > 1$ at $r = 0$ take the form

$$S_d\left(0, \frac{\beta e^2}{\lambda_{ei}}\right) \approx \pi^{1/2}\left(\frac{\beta e^2}{\lambda_{ei}}\right)^3 n_0^{-3}\exp\left(\frac{\beta e^2}{n_0^3}\right),$$
$$S_c\left(0, \frac{\beta e^2}{\lambda_{ei}}\right) \approx 2\pi^{1/2}\frac{\beta e^2}{\lambda_{ei}}. \tag{15}$$

At $n_0 \geq 100$, it will suffice to use (14) and (15) and the hydrogen wave functions and energy levels to determine the potential $\Phi_{ei}(r, T)$. When determining $\Phi_{ei}(r, T)$ for the Xe ion, we must also take into account the fact that its size is finite (its crystallographic radius is about 2 Å). Figure 1 shows the electron–ion pseudopotentials at $T = 0.1$, 0.5, and 1 K and, for comparison, the Coulomb potentials.

4.2. The Electron–Electron and Ion–Ion Pseudopotentials

The Slater partition function for the interaction between two electrons is [21]

$$S_{ee}(r, T) = 16\pi^{3/2}\lambda_{ee}^3 \sum_\alpha |\Psi_\alpha(r, \sigma_1, \sigma_2)|^2 \exp(-\beta E_\alpha) \equiv \exp(-\beta\Phi_{ee}(r, T)). \tag{16}$$

The wave functions in expression (16) depend on the electron spins σ_1 and σ_2 and must be antisymmetric. Expression (16) can be written as a sum of the contributions from the wave functions with symmetric and nonsymmetric parts:

$$S_{ee}(r, T) = \frac{1}{4}S_{ee}^c(r, T) + \frac{3}{4}S_{ee}^a(r, t) \equiv \exp(-\beta\Phi_{ee}(r, T)). \tag{17}$$

The potential $\Phi_{ee}(r, T)$ was numerically calculated by Barker [22] over a wide temperature range, $T = 10^2$–10^5 K. He suggested the following fitting formula for $\Phi_{ee}(r, T)$:

$$\Phi_{ee}(r, T) = \frac{2}{r}(1 - \exp(-8.35 \times 10^{-4} r T^{0.625})),$$
$$\Phi_{ee}(0, T) = 16.7 \times 10^{-4} T^{0.625}, \quad (18)$$

where r is measured in a_0, T is in Kelvins, and Φ_{ee} is in Rydbergs (Re = $0.5me^4/\hbar^2$).

At long range, formula (18) is identical to the Coulomb law. For $\beta e^2/\lambda_{ee} > 1$, expression (17) at $r = 0$ can be written [23] as

$$S_{ee}\left(0, \frac{\beta e^2}{\lambda_{ee}}\right) \approx \left(\frac{4\pi}{3}\right)^{1/2} \left(\frac{\beta e^2}{\lambda_{ee}}\right)^{4/3} \times \left(\frac{\pi}{2}\right)^{1/3} \exp\left(-3\left(\pi \frac{\beta e^2}{2\lambda_{ee}}\right)^{2/3}\right). \quad (19)$$

Thus, for $\beta e^2/\lambda_{ee} > 1$, fit (18) can be used down to $T = 0.1$ K.

Figure 2 shows the electron–electron pseudopotentials at $T = 0.1$, 0.5, and 1 K and, for comparison, the Coulomb potentials.

According to [21], the expressions for the ion–ion pseudopotentials are identical to the Coulomb law. We must only take into account the fact that the ion size (e.g., the crystallographic radius) is finite.

5. CALCULATING THE THERMODYNAMIC QUANTITIES AND CORRELATION FUNCTIONS

5.1. The Method of Calculation

In the pseudopotential approach, the quantum partition function reduces to an expression that is classical in form [21]. Therefore, all of the methods developed in the statistical thermodynamics of classical systems (both analytical and numerical) can be used to determine the relevant thermodynamic quantities.

We used the Monte Carlo method for a multicomponent plasma in a canonical ensemble developed in [24, 25] to calculate the thermodynamic quantities and correlation functions of an ultracold Rydberg plasma.

In this case, determining the various thermodynamic quantities reduces to calculating the mean values of the known functions of coordinates q. For example, for the energy, we obtain

$$\bar{E} = Q^{-1}(N, V, T) \int_V \ldots \int E_N(q) S_N(a, T) d^N q, \quad (20)$$

where $Q(N, V, T)$ is the path integral.

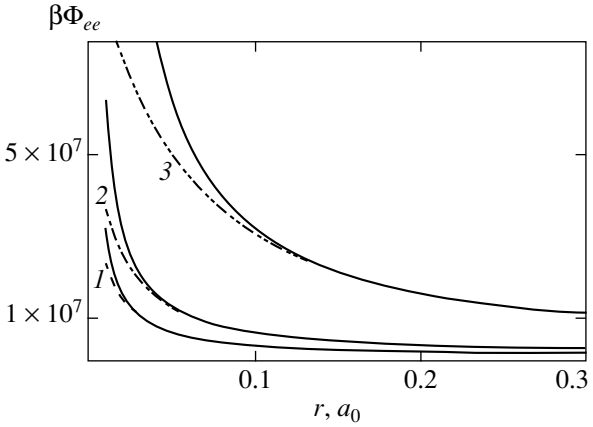

Fig. 2. The electron–electron pseudopotentials at various temperatures, $T = 1$ (*1*), 0.5 (*2*), and 0.1 K (*3*), compared to the Coulomb potentials (solid lines).

The Monte Carlo method is a numerical method that uses Markov chains [24]. It allows us to select only the principal, most typical terms that define the integral sum. Therefore, it is also called a method of significant selection. Another peculiarity of the method is the use of periodic boundary conditions. The entire three-dimensional space is broken down into equal cells of volume V with N particles in each cell. If one of the particles exits from a cell due to a change in its coordinates, then its image from a neighboring cell simultaneously enters through the opposite cell face, and the number of particles in the cell is conserved.

The errors in the Monte Carlo results [24] are attributable to the choice of the number of particles in the cell and to the finite length of the Markov chain. To estimate the error in choosing the number of particles, we performed calculations for various $N = 16$, 32, 64, and 128 and showed convergence ($(\propto N^{-1})$). Our estimate of the statistical error due to the finite length of the Markov chain [24] allowed us to choose Markov chains of the required length. In addition, we discarded the nonequilibrium part. We also calculated the electron–electron, $g_{ee}(r)$, ion–ion, $g_{ii}(r)$, and electron–ion, $g_{ei}(r)$, radial correlation functions.

5.2. Results of the Calculations

Thus, we consider the pseudopotential model of an ultracold Rydberg plasma. Experimental data suggest that this plasma consists of electrons, singly charged ions, and atoms in highly excited ($n > 100$) states. There are no low-excitation ($n < 100$) states in this plasma, because it was produced through the laser excitation of atoms at a certain wavelength, and because an anomalous increase in the recombination time was observed in the experiment.

We performed calculations for the temperature range $T = 0.1$–10 K and the density range $n = 10^{-2}$–10^{16} cm^{-3}. The calculations in the range of low densities

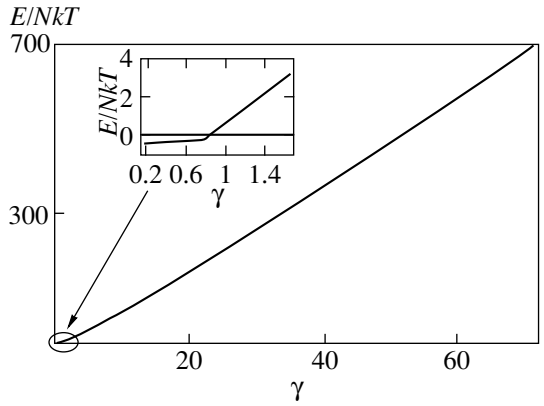

Fig. 3. Internal energy per particle, *E*/*NkT*, versus nonideality parameter γ.

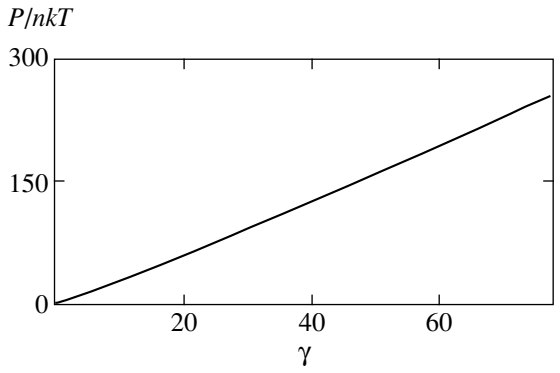

Fig. 4. Pressure *P*/*nkT* versus nonideality parameter γ.

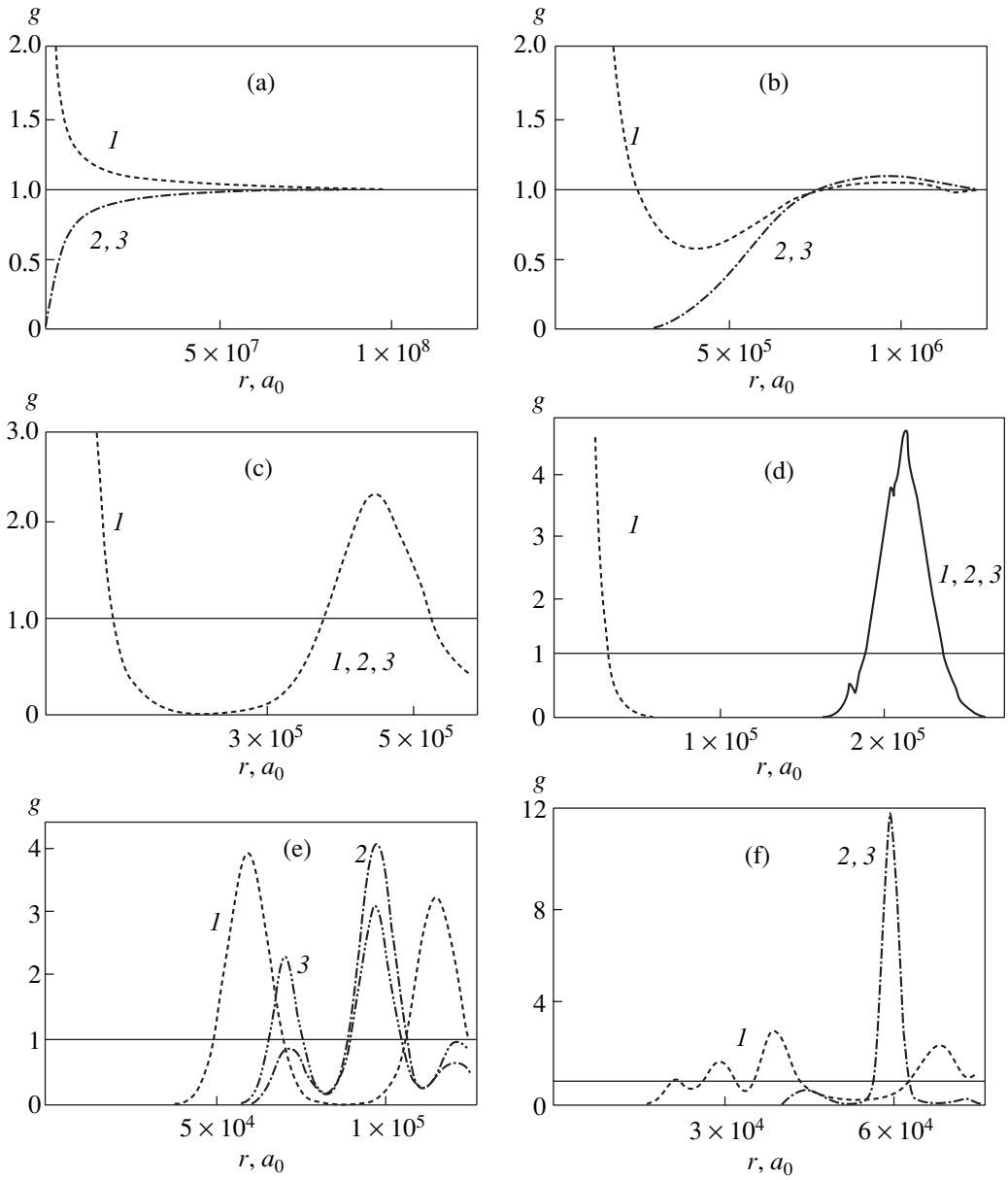

Fig. 5. The correlation functions at various densities and temperature $T = 0.1$ K: $g_{ei}(r)$ (*1*), $g_{ee}(r)$ (*2*), and $g_{ii}(r)$ (*3*); (a) $n = 10$, $\gamma = 0.036$; (b) $n = 10^7$, $\gamma = 3.6$; (c) $n = 10^8$, $\gamma = 7.7$; (d) $n = 10^9$, $\gamma = 16.7$; (e) $n = 10^{10}$, $\gamma = 36$; and (f) $n = 10^{11}$, $\gamma = 77$.

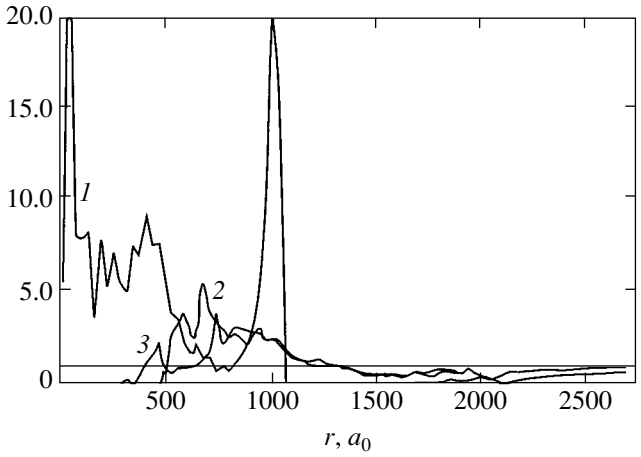

Fig. 6. The correlation functions at density $n = 10^{15}$ cm^{-3} and temperature $T = 10$ K: $g_{ei}(r)$ (*1*), $g_{ee}(r)$ (*2*), and $g_{ii}(r)$ (*3*).

were needed to pass to the limit of the values that are consistent with the Debye–Hückel approximation for $\gamma \ll 1$ (see, e.g., [21]).

In Figs. 3 and 4, internal energy E/NkT per particle and pressure P/nkT are plotted against nonideality parameter γ. In the limit of small γ, there is agreement with the Debye–Hückel approximation (see the inset in Fig. 3). At $\gamma < 0.5$, the dimensionless energy E/NkT reaches the Debye value

$$\frac{E}{NkT} = -\sqrt{\pi}\gamma^{3/2}. \quad (21)$$

Figures 5 and 6 show the correlation functions $g_{ee}(r)$, $g_{ii}(r)$, and $g_{ei}(r)$ for various densities and temperatures $T = 0.1$ and 10 K, respectively. For $\gamma \ll 1$, there is good agreement with the Debye–Hückel approxima-

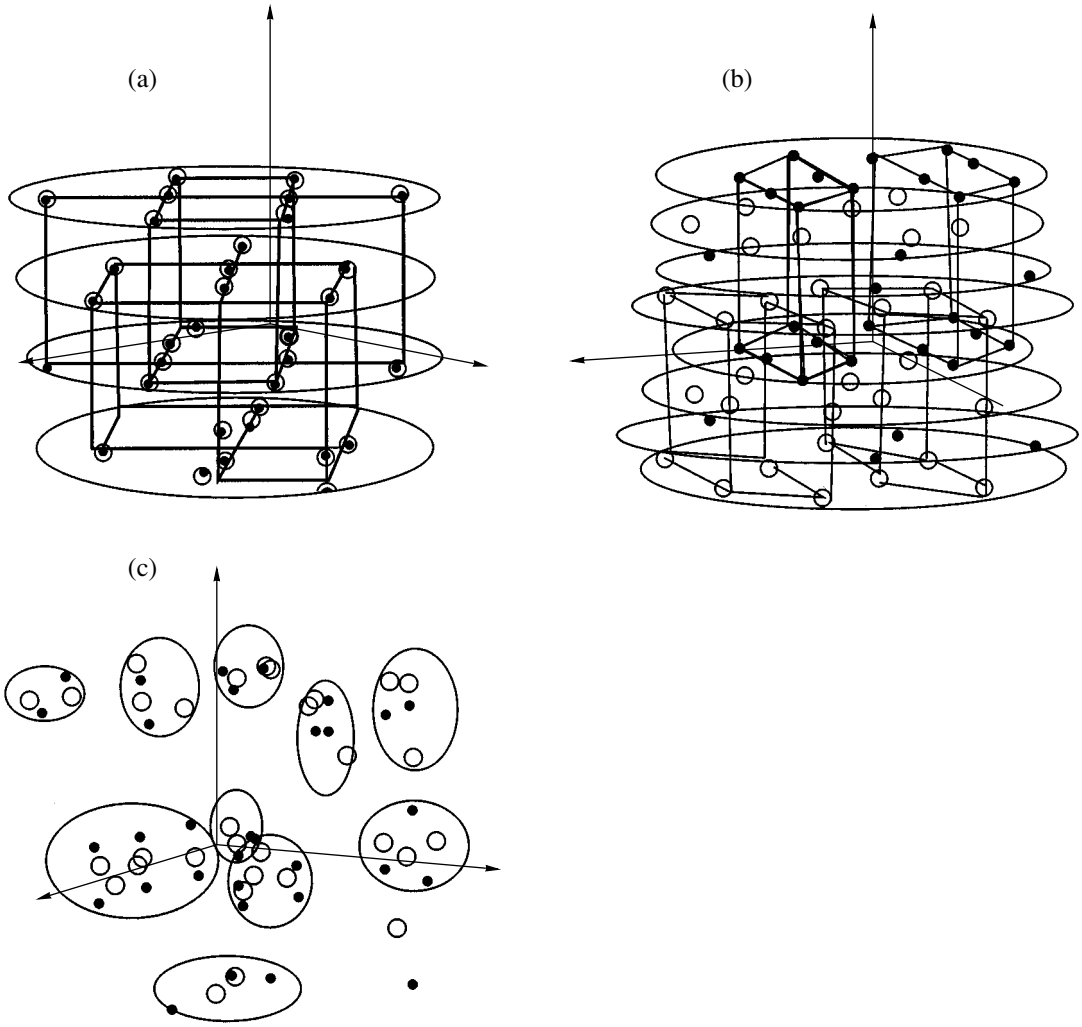

Fig. 7. The graphical images of the particle coordinates that correspond to the correlation functions $g_{ee}(r)$, $g_{ii}(r)$, and $g_{ei}(r)$. The open and filled circles represent the ions and electrons, respectively: (a) $T = 0.1$ K, $n = 10^9$ cm^{-3}, the ions and electrons are at the lattice site; (b) $T = 0.1$ K, $n = 10^{10}$ cm^{-3}, the ions are at the sites of one lattice, while the electrons are at the sites of the other lattice; (c) $T = 10$ K, $n = 10^{15}$ cm^{-3}, the ions and electrons form droplets with lattice site nuclei, the transition state between the short-range order and the lattice.

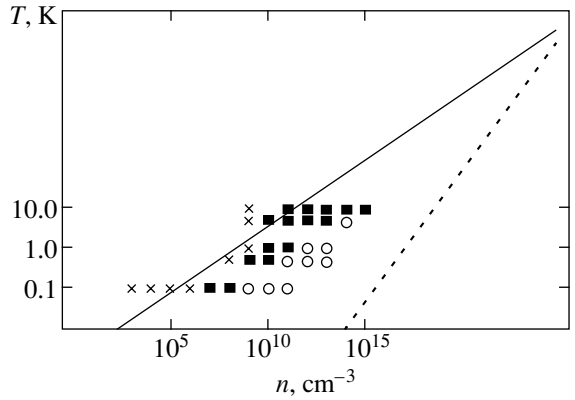

Fig. 8. The *n–T* diagram. The crosses, squares, and circles represent the gaseous, liquid, and solid (lattice) states of the plasma, respectively. The solid and dashed lines correspond to $\gamma = 1$ and $n\lambda^3 = 1$, respectively.

tion (linearized or nonlinearized). For $\gamma \geq 1$, the shape of the correlation functions suggests that a short-range order is formed among particles of both the same and opposite signs. This order is enhanced with increasing γ. The maxima of the correlation functions increase, while their minima become zero, which is attributable to the formation of a strict order in the spatial arrangement of particles. There are almost no particles in the region of zero correlation functions.

We used a visualization program to better understand the situation related to ordering with increasing γ. This program visualizes the arrangement of particles in various equilibrium configurations. Figures 7a–7c show some of the equilibrium configurations for various T and n.

Let us discuss the results for the $T = 0.1$ K isotherm. The order that corresponds to a lattice of size $L = 2.2 \times 10^5 a_0$ at $n = 10^9$ cm^{-3} arises as the density increases (Figs. 5d and 7a). The pairs of electrons and ions are located at the lattice sites at distance $r = 2.2 \times 10^5 a_0$. As the density increases to $n = 10^{10}$ cm^{-3} (Figs. 5e and 7b), the electrons and ions that form the pair move apart, and two (electron and ion) lattices are formed. This probably suggests that two nested lattices constituted the initial lattice at the sites of which the pairs were located.

As the temperature increases, the formation of an ordered structure shifts toward higher particle densities. Thus, for $T = 10$ K and at a much higher density, $n = 10^{15}$ cm^{-3}, only a short-range order in the form of electron–ion clusters (as we see from the equilibrium configuration) shown in Figs. 6 and 7c is established. These clusters are droplets of oppositely charged particles, with the electrons and ions in these droplets lining up in minilattices.

As was noted above, the energy E/NkT at $\gamma \geq 0.1$ in the range $T = 0.1$–10 K is a linear function of γ (see Fig. 3). This implies that, eliminating the temperature from this function, we will obtain an expression similar to the standard Madelung law for an ionic crystal [30]:

$$\frac{E}{N} = Ae^2 n^{1/3}, \tag{22}$$

where $A = 8$–9 is a constant (an analogue of the Madelung constant).

As follows from our calculations, the lattice constant is proportional to $n^{-1/3}$. The form of Eq. (22) suggests that an order similar to a crystal lattice is established in the ionized gas produced at $\gamma \geq 1$. In this case, the energy is a function of the mean particle separation, which is approximately equal to the lattice constant.

Figure 8 shows an *n–T* diagram. The region of parameters that corresponds to a Debye plasma is indicated by crosses; the regions where droplets and lattices appear are indicated by squares and circles, respectively. The $\gamma = 1$ and $n\lambda^3 = 1$ lines are also shown in the figure. We see from this diagram that the formation of a short-range order begins only at $\gamma \approx 1$; as was described above, the formation of an ordered structures shifts toward higher particle densities as the temperature increases. In addition, under the given conditions, a long-range order is formed long before the onset of degeneracy.

Our results also give us an insight into what the authors of [1–3] call the anomalously slowed down recombination. There are no Rydberg atoms that must recombine in an ionized gas at $\gamma \geq 1$. However, there is a short-range order (and a long-range order at $\gamma \gg 1$) for charged particles of both the same and opposite signs, which reduces the probability of the approach and recombination of oppositely charged particles.

6. CONCLUSIONS

We have considered a Rydberg ionized gas formed from continuum electrons and ions. We investigated the temperature range $T = 0.1$–10 K and the density range $n = 10^{-2}$–10^{16} cm^{-3}. As a result, we found the formation of a structure at $\gamma \geq 1$, which probably leads to the experimentally observed slowdown of the recombination. The structure is formed in the region where the electron gas is far from being degenerate ($n\lambda^2 \ll 1$) and where the structure itself changes from a short-range order (similar to the structure in a liquid) to a long-range order (similar to the lattice in solid bodies). Adding states of the discrete spectrum to the gas under consideration will change the properties of this gas. When these states are taken into account for specific densities and temperatures, the energy decreases, which may cause the phase diagram to change.

The suggested model contains no specific parameters of the elements. Therefore, it may be used for a gas of any element.

ACKNOWLEDGMENTS

This work was supported in part by the Russian Foundation for Basic Research (project nos. 02-02-16320 and 04-02-17474).

REFERENCES

1. T. C. Killian, S. Kulin, S. D. Bergeson, *et al.*, Phys. Rev. Lett. **83**, 4776 (1999).
2. S. Kulin, T. C. Killian, S. D. Bergeson, and S. L. Rolston, Phys. Rev. Lett. **85**, 318 (2000).
3. T. C. Killian, M. J. Lim, S. Kulin, *et al.*, Phys. Rev. Lett. **86**, 3759 (2001).
4. L. Spitzer, Jr., *Physics of Fully Ionized Gases*, 2nd ed. (Wiley, New York, 1962; Mir, Moscow, 1957), p. 35.
5. E. M. Lifshitz and L. P. Pitaevskiĭ, *Physical Kinetics* (Nauka, Moscow, 1979; Pergamon Press, Oxford, 1981).
6. É. A. Manykin, M. I. Ozhovan, and P. P. Poluéktov, Dokl. Akad. Nauk SSSR **260**, 1096 (1981) [Sov. Phys. Dokl. **26**, 974 (1981)].
7. É. A. Manykin, M. I. Ozhovan, and P. P. Poluéktov, Zh. Éksp. Teor. Fiz. **84**, 442 (1983) [Sov. Phys. JETP **57**, 256 (1983)].
8. É. A. Manykin, M. I. Ozhovan, and P. P. Poluéktov, Zh. Éksp. Teor. Fiz. **102**, 804 (1992) [Sov. Phys. JETP **75**, 440 (1992)].
9. C. Aman, J. B. C. Pettersson, and L. Holmlid, Chem. Phys. **147**, 189 (1990).
10. R. S. Svensson, L. Holmlid, and L. Lundgren, J. Appl. Phys. **70**, 1489 (1991).
11. C. Aman, J. B. C. Pettersson, H. Lindroth, and L. Holmlid, J. Mater. Res. **7**, 100 (1992).
12. É. A. Manykin, M. I. Ozhovan, and P. P. Poluéktov, Khim. Fiz. **18**, 88 (1999).
13. R. Svensson and L. Holmlid, Phys. Rev. Lett. **83**, 1739 (1999).
14. V. I. Yarygin, V. N. Sidel'nikov, I. I. Kasikov, *et al.*, Pis'ma Zh. Éksp. Teor. Fiz. **77**, 330 (2003) [JETP Lett. **77**, 280 (2003)].
15. G. É. Norman, in *Proceedings of XVI International Conference on Impact of Intensive Energy Fluxes on the Matter*, Ed. by V. E. Fortov (Inst. Probl. Khim. Fiz. Ross. Akad. Nauk, Chernogolovka, 2001), p. 110.
16. G. É. Norman, Pis'ma Zh. Éksp. Teor. Fiz. **73**, 13 (2001) [JETP Lett. **73**, 10 (2001)].
17. A. N. Tkachev and S. I. Yakovlenko, Kvantovaya Élektron. (Moscow) **30**, 1077 (2000).
18. A. N. Tkachev and S. I. Yakovlenko, Pis'ma Zh. Éksp. Teor. Fiz. **73**, 71 (2001) [JETP Lett. **73**, 66 (2001)].
19. B. B. Zelener, B. V. Zelener, and É. A. Manykin, in *Proceedings of XVII International Conference on Equations of State of Substance*, Ed. by V. E. Fortov (Inst. Probl. Khim. Fiz. Ross. Akad. Nauk, Chernogolovka, 2002).
20. V. S. Filinov, E. A. Manykin, B. B. Zelener, and B. V. Zelener, in *Proceedings of 12th International Laser Physics Workshop* (Hamburg, 2003).
21. B. V. Zelener, G. É. Norman, and V. S. Filinov, *Perturbation Theory and Pseudopotential in Statistical Thermodynamics* (Nauka, Moscow, 1981), p. 101.
22. A. A. Barker, J. Chem. Phys. **55**, 1751 (1971).
23. V. S. Vorob'ev, G. É. Norman, and V. S. Filinov, Zh. Éksp. Teor. Fiz. **57**, 838 (1969) [Sov. Phys. JETP **30**, 459 (1969)].
24. V. M. Zamalin, G. É. Norman, and V. S. Filinov, *The Monte Carlo Method in Statistical Thermodynamics* (Nauka, Moscow, 1977), p. 129.
25. V. S. Filinov, M. Bonitz, W. Ebeling, and V. E. Fortov, Plasma Phys. Controlled Fusion **43**, 743 (2001).
26. V. S. Filinov, M. Bonitz, P. Levashov, *et al.*, J. Phys. A: Math. Gen. **36**, 6069 (2003).
27. V. S. Filinov, V. E. Fortov, M. Bonitz, and P. R. Levashov, Pis'ma Zh. Éksp. Teor. Fiz. **74**, 422 (2001) [JETP Lett. **74**, 384 (2001)].
28. V. S. Filinov, V. E. Fortov, and M. Bonitz, Pis'ma Zh. Éksp. Teor. Fiz. **72**, 361 (2000) [JETP Lett. **72**, 245 (2000)].
29. V. S. Filinov, V. E. Fortov, M. Bonitz, and D. Kremp, Phys. Lett. **274**, 228 (2000).
30. C. Kittel, *Introduction to Solid State Physics*, 5th ed. (Wiley, New York, 1976; Nauka, Moscow, 1978).

Translated by V. Astakhov